Ablation of Red Stable Transfected Prostate Cancer Cell Lines by C-CPE Gold-Nanoparticle Mediated Laser Intervention

Suhayla Alnajjar
University of Veterinary Medicine Hanover https://orcid.org/0000-0002-8158-7602
Ingo Nolte
University of Veterinary Medicine Hannover: Tierarztliche Hochschule Hannover
Annegret Becker
Leibniz Universität Hannover: Leibniz Universitat Hannover
Tina Kostka
University of Veterinary Medicine Hannover: Tierarztliche Hochschule Hannover
Jan Torben Schille
University of Veterinary Medicine Hannover: Tierarztliche Hochschule Hannover
Sina Sender
Universitatsmedizin Rostock
Simon Villa Perez
Universitätsmedizin Rostock: Universitatsmedizin Rostock
Marcus Frank
Rostock University Medical Center: Universitatsmedizin Rostock
Anaclet Ngezahayo
Leibniz Universitat Hannover
Hugo Murua Escobar (hugo.murua.escobar@med.uni-rostock.de)
University of Rostock https://orcid.org/0000-0001-7123-7986

Research article

Keywords: Cell line, red fluorescent protein, C-CPE, gold nanoparticle, GNOME-LP

Posted Date: April 1st, 2021

DOI: https://doi.org/10.21203/rs.3.rs-378422/v1

Abstract

Background: Claudin (CLDN) proteins have been described to be found and accordingly targeted to evaluate novel therapeutic approaches. C-terminus of *Clostridium perfringens* enterotoxin (C-CPE) binds efficiently several claudins and thus recombinant C-CPE conjugated to gold nanoparticles (AuNPs) has been used for cancer cell targeting using gold nanoparticle- mediated laser perforation (GNOME-LP). Cancer cells inoculation is routinely used to generate *in vivo* models to evaluate novel therapeutic approaches in prostate cancer. However, detailed characterization of cancer spreading and early tumor development and therapeutic response is often limited as conventional cell lines do not allow advanced deep tissue imaging.

Methods: two canine prostate cancer cell lines were stably transfected with red fluorescent protein (RFP), followed by G418 selection. RFP marker as well as CLDN3, -4 and -7 expression was comparatively confirmed by flow cytometry, qPCR and immunofluorescences. For cancer cells targeting, GNOME-LP at a laser fluence of 72 mJ/cm² and a scanning speed of 0.5 cm/s was used.

Statistical analysis was performed using SAS software 7.1, Dunnett´s Multiple Comparison Test and Student´s two-sided t-test. Differences were considered statistically significant for $p<0.05$.

Results: we established two canine prostate carcinoma cell lines, stably expressing RFP allowing perspective deep tissue imaging. Directed C-CPE-AuNP binding to native and RFP transfected cells verified the capability to specifically target CLDN receptors. Cancer cell ablation was demonstrated *in vitro* setting using a combination of gold nanoparticle mediated laser perforation and C-CPE-AuNPs treatment reducing tumor cell viability to less than 10 % depending on cell line.

Conclusion: the results confirm that this therapeutic approach can be used efficiently to target prostate carcinoma cells carrying a marker protein allowing deep tissue imaging. The established cell lines and the verified proof of concept *in vitro* study provide the basis for perspective Xenograft model *in vivo* studies.

The introduce red fluorescence enables deep tissue imaging in living animals and therefore detailed characterization of tumor growth and subsequently possible tumor ablation through C-CPE-AuNPs treatment.

Background

Advanced experimental approaches in cancer research require the establishment of tumor specific *in vivo* animal models. Therefore, cell lines represent a powerful tool allowing the generation of neoplasia mimicking closely the initial tumors through xenografts [1, 2]. Within these models, the characterization of tumor development and the possibility to monitor tumor cell migration is of major interest for the evaluation of novel therapeutics. Fluorescent proteins and bioluminescent systems provide unique opportunities for non-invasive labeling and tracking of specific cell types in living organisms in real time.

Together with the development of new systems for whole-body imaging, fluorescent proteins can be used to visualize many types of cancer processes, including primary tumor growth, tumors cell motility and invasion, metastases and the interaction between tumor and its microenvironment (tumor–host interaction) [3–5]. For deep imaging of animal tissues, the optical window favorable for light penetration is in near-infrared wavelengths, which are less absorbed by tissue, requiring proteins with emission spectra in the far-red wavelengths [3, 5–9]. Tumor cell lines stably expressing detectable fluorescent proteins enable to evaluate the efficacy of therapeutic anticancer treatments through whole-body imaging without the need for any invasive procedures in tumor-bearing xenograft models.

Claudins (CLDNs) are proteins abnormally regulated in different human and animal neoplasms affecting the mammary gland, prostate, pancreas, and colon [10–16]. CLDN family consists of more than 20 proteins essential for tight-junction formation in epithelial and endothelial cells. Additionally, CLDNs are important regulators of paracellular transport and maintenance of cell polarity [10, 16–19].

The second extracellular loop of CLDN3, -4 and − 7 acts as a receptor for the *Clostridium perfringens* enterotoxin (CPE) [20–23]. The C-terminal domain of CPE (C-CPE) by itself retains its high-affinity binding to CLDN, but overcomes the toxic drawback of full-length CPE, which limited its use to local therapy. Considering C-CPE's ability to modulate the tight-junction, and thus the barrier function of epithelium and endothelium in a non-cytotoxic way, C-CPE has emerged as a promising therapeutic agent [24–26] .

In recent years, laser therapy using gold nanoparticles (AuNPs) has rapidly evolved as a non-invasive thermotherapy for cancer as it enables hyperthermia of tumor tissues [27–31]. During laser treatment, AuNPs are delivered into tumors and are irradiated with laser light. AuNPs absorb light energy, causing electron excitation and subsequent non-radiative relaxation. The absorbed light is converted into heat, which irreversibly develops cell membrane disruption or protein denaturation of the surrounding tumor cells [28, 32] .

Although AuNPs can passively accumulate in cancer cells [33], they have a non-specific connection with cell membranes [32, 34]. Due to the AuNPs accumulation in normal cells, an undesirable damage is associated with non-targeted AuNPs [35]. In a previous study, we demonstrated that C-CPE-AuNPs can be used to specifically and efficiently kill human colon, conventional mammary gland and esophageal adenocarcinoma cells, expressing CLDN3, -4 and − 7, using gold nanoparticle-mediated laser perforation (GNOME-LP) technique [36, 37] .

Aside from humans, dogs are the only animal known to naturally develop prostate cancer [38]. In both species, adenocarcinomas of the prostate represent an age-dependent, locally invasive disease [39, 40] with dysregulated CLDN expression [41–45]. Human and canine prostate carcinomas are at present incurable once they have metastasized. Since metastases are highly resistant to current conventional therapies, new therapeutic strategies are necessary. Considering the similarities concerning the presentation of the disease between both species, canine prostate cancer is considered a reliable model for the testing of novel therapies for castrate-resistant prostate cancer in humans [46]. Consequently, data obtained in dogs may also lead to progress in human tumor research.

Herein we established and characterized stable red fluorescent canine prostate tumor cell lines, which provide a novel tool for *in vitro* and *in vivo* tumor imaging. Further we characterized if the fluorescent emission interferes with conventional laser ablation and optimized the therefore required parameters *in vitro*. Finally, selective C-CPE AuNPs ablation using GNOME-LP in combination was used to eliminate prostate CLDN3, -4 and/or -7 expressing tumor cell lines.

Materials And Methods

Cell lines and culture

Canine tumor cell lines TihoDProCarc0840 (DT0840) and TihoDProAdCarc0846 (DT0846) were previously derived by our group from canine prostate carcinomas. DT0840 was generated from a 10-year-old Pit Bull Terrier, castrated [47] and DT0846 was generated from a 6.3-year old intact German Rough Haired Pointer [48]. Both cell lines have been demonstrated to express CLDN3, -4 and − 7 [41].

The cells were cultivated separately in 25 cm^2 cell culture flasks in medium 199 (Gibco by Life Technologies, Darmstadt, Germany) supplemented with 10% Fetal Bovine Serum (FBS Superior, Biochrom GmbH, Berlin, Germany) and 2% penicillin/streptomycin (Biochrom GmbH, Berlin, Germany), and incubated in a humidified incubator maintained at 37 ˚C with 5% CO_2. Cultivation medium was replaced twice per week.

Red fluorescence expression plasmid

For transfection, the pFusionRed-C (Evrogen, Moscow, Russia) plasmid was used. The vector encodes for red fluorescent protein FusionRed as well as a neomycin resistance gene allowing selection of stably transfected cells using Geneticin® Selective Antibiotic (G418) (Life Technologies, Darmstadt, Germany). The vector was inserted into *E. coli* DH5α competent cells according to standard heat shock transformation procedures for further multiplication. Expanded Plasmid DNA was extracted from bacteria culture using Nucleo Bond® PC 500 plasmid DNA purification Kit (MACHEREY-NAGEL GmbH, Düren, Germany).

Transfection of canine tumor cell lines

Both cell lines were seeded with a density of $5*10^5$ cells in 6-well plates 24 hours before transfection. The transfection was performed according to the manufacturer's protocol using 6 µl X-treme GENE HP DNA Transfection Reagent (Roche GmbH, Mannheim, Germany) in 200 µl serum-reduced Opti-MEM I media (Life Technologies, Darmstadt, Germany) containing 2.5 µg of the isolated and purified pFusionRed-C plasmid. The transfection complex remained for 20 min at room temperature. After adding the transfection complex to the respective cells, the plates were incubated in a humidified 5% CO_2 incubator for 48 hours at 37 °C. The expression of the fluorescent protein was verified using a Leica DMI 6000B fluorescence microscope (Leica Microsystem GmbH, Wetzlar Germany).

Geneticin® selective antibiotic kill curve assay

The titration of a suitable amount of antibiotics required for the selection of DT0846 and DT0840 cell lines was performed using a kill curve assay. Different G418 concentrations (0, 100, 200, 400, 600, 800, 1000 µg/ml) were applied on 100,000 native DT0846 and DT0840 cells, seeded in 12-well plates. For the selection of positive cells after transfection, the lowest concentration was chosen in which no non-transfected cell survived after seven days of G418 exposure determined by microscopy and flow cytometry analysis.

Selection of positively transfected cells

One day after transfection, the cultivation medium 199 was replaced with medium 199 containing antibiotic G418. A concentration of 200 µg/ml G418 was used for both transfected cell lines. Subsequently, the selection medium was changed every 48 hours for the first two weeks, which led to the selection of cells that stably integrated the FusionRed plasmid, with the encoded antibiotic resistance gene, into their genomic DNA. Accordingly, cells not expressing the construct were killed by G418.

Fluorescence microscopy and flow cytometry

During the selection of transfected cell lines by Geneticin (G418), cells were controlled by fluorescence microscopy weekly. FusionRed expression of the transfected cell lines was quantified in a MACSQuant flow cytometer monthly (MACS Miltenyi Biotec, Bergisch Gladbach, Germany). Cells were detached with Tryp-LE™ Express (Gibco by Life Technologies) into single-cell suspension, adjusted to $1*10^6$ cells in 500 µl phosphate-buffered saline (PBS), and examined using the PE channel in a flow cytometer. Results were analyzed with FlowJo Version 7.6.5 (FlowJo, Ashland, OR, USA). Transfected cell lines were used for all further experiments when overcoming passage 50.

In vitro imaging using the NightOWL LB 983 *in vivo* imaging system

Viable cells were harvested, counted and plated at a density of 2.5×10^6 per well in a 96-well plate and followed by a 1:2 serial dilution until 0.156×10^6 cells per well in duplicates. Each well was set to a volume of 250 µl. Unlabeled pre-B-ALL NALM-6 cells were used as controls in equivalent concentrations. The plate was incubated overnight and images were taken with the NightOWL LB 983 imaging system (Berthold Technologies, Bad Wildbad, Germany). As settings, an excitation filter of 525 nM and emission filter of 655 nM with variable exposure times (4 s/10 s) were used. Images were analyzed with the indiGO software (Berthold Technologies, Bad Wildbad, Germany).

RNA isolation and cDNA synthesis

Total RNA was isolated from transfected and native prostate tumor cell lines using the RNeasy®Mini Kit RNA Purification (Qiagen, Hilden, Germany) according to the manufacturer´s instruction. RNA isolation was performed three times per cell line. DNase digestion was carried out with RNase-Free DNase Set (Qiagen) to avoid genomic DNA contamination. Subsequently, cDNA synthesis was performed using

Transcriptor First Strand cDNA Synthesis Kit (Roche, Mannheim, Germany), 1000 ng of total RNA, and anchored-oligo $(dt)_{18}$ primer according to the manufacturer´s instructions.

Quantitative real-time RT-PCR

To verify expression of *CLDN* genes after transfection process, transfected and native prostate tumor cell lines were comparatively analyzed by quantitative PCR. Primer pairs for *CLDN3, CLDN4*, and *CLDN7* were designed according to the mRNA sequences given by the National Center for Biotechnology Information (NCBI) (Table 1). Real-time PCR was performed using Fast SYBR™ Green Master mix Kit (Life Technologies, Darmstadt, Germany) according to the manufacturer´s instructions. Quantitative PCR reactions were carried out in real-time PCR cycler peqSTAR 96q (PEQLAB Biotechnologies GmbH, Erlangen, Germany). The qPCR results were analyzed using the delta-delta CT (ΔΔCT) method relative to non-transfected cells. Mean values of three wells were used per measured gene. Normalization was done against housekeeping genes beta-actin (*ACTB*) and glyceraldehyde 3-phosphate dehydrogenase (*GAPDH*). The experiment was performed three times.

Table 1
Primer sequences used for real-time PCR.

Target gene	Forward primer sequence	Revers primer sequence	Accession Number
CLDN3	5’ gcccaccaagatcgtctact 3’	5’ gtctggagtgggttggtctc 3’	NM_001003088.1
CLDN4	5’ gcctcacttacccacctgac 3’	5’ accagtttgtggcaccttca 3’	XM_005620962.3
CLDN7	5’ cacgatgggcatgaagtgta 3’	5’ taccaaggcagcaagacctc 3’	XM_546584.5
ACTB	5’ tcgctgacaggatgcagaag 3’	5’ gtggacagtgaggccaggat 3’	NM_001195845.2
GAPDH	5’ cagtatgattctacccacggcaa 3’	5’ cctggaagatggagatggactt 3’	NM_001003142.2

Immunofluorescence assay

Immunofluorescence was performed for native and transfected cell lines to further confirm CLDN expression. The cells were cultivated on rat collagen type I (Trevigen, Gaithersburg, MD, USA) coated glass coverslips. Thereafter, cells were washed with PBS, fixed wit (1:1) Acetone/Methanol for 5 min at -20 °C and blocked for 30 min with 1% BSA (bovine serum albumin, Sigma-Aldrich, Taufkirchen, Germany) in PBS at 37 °C. CLDNs were stained with primary antibodies (Table 2) diluted in PBS containing 1% BSA, overnight at 4 °C. Cells were washed with PBS. iFlour™ 488 Anti-mouse (AAT Bioquest, CA, USA) and iFlour™ 555 Anti-rabbit (AAT Bioquest, CA, USA) were diluted 1:500 in PBS containing 1% BSA and added to the respective cells as secondary antibodies for 1 h at 37 °C. For nuclei staining, DAPI (2 µM) (Sigma-Aldrich) was used. Cells were stored in PBS at 4 °C for further analysis. As a control for unspecific binding sites, cells were also incubated with only the secondary antibodies. Fluorescent images of cells were taken with a Nikon Eclipse TE2000-E confocal laser scanning microscope (400 nm for DAPI, 555 nm for

CLDN3 and − 7 proteins and 488 nm for CLDN4), with a 60x water immersion objective and software EZ-C1 3.80 (Nikon, Düsseldorf, Germany).

Table 2
Primary Antibodies used for immunofluorescence assays.

Protein	Antibody	Concentration
CLDN3	Rabbit anti-mouse CLDN3 34-1700 (Thermo Fischer Scientific, Waltham, MA, USA)	3 µg/ml
CLDN4	Mouse anti-human CLDN4 34-1700 (Thermo Fischer Scientific)	3 µg/ml
CLDN7	Rabbit anti-human CLDN7 32-9400 (Thermo Fischer Scientific)	2 µg/ml

Visualization of C-CPE-CLDN binging

The *C. perfringens* enterotoxin C-terminal fragment (C-CPE) with an N-terminal Strep-tag II was prepared as described previously. For C-CPE-CLDN binding visualization, the C-CPE was conjugated to green fluorescent Strep-Tactin® Chromeo 488 dye (IBA, Goettingen, Germany). The complex was generated freshly before usage, by mixing 2.5 µl Strep-Tactin® Chromeo 488 (0.5 mg/mL) as recommended by the manufacturer with C-CPE dissolved in elution buffer. The mix was incubated overnight at 4 °C to allow binding of C-CPE with Strep-Tactin® Chromeo 488. To reach a final concentration of 20 µg/ml C-CPE, the mixture was diluted with 250 µl culture medium. Cells were cultured in a monolayer and stained for 3 h at 37 °C with 20 µg/ml C-CPE-Chromeo 488 complex. For nuclei staining, 1 µM Hoechst 33258 (Sigma-Aldrich) was used. Thereafter, cells were fixed with 4% formaldehyde for 10 min at room temperature and stored in PBS at 4 °C. The cells were imaged with a Nikon Eclipse TE2000-E confocal laser scanning microscope (346 nm for Hoechst 33258 and 488 nm for Chromeo 488) with a 60x water immersion objective and software EZ-C1 3.80 (Nikon).

Tumor cells ablation by GNOME-LP and C-CPE-AuNPs complex interaction

For tumor cell killing using a laser beam, confluent cells in 96-wells were treated with the C-CPE-AuNPs complex for 3 h in a cell culture incubator to allow adhesion of the complex onto the cells. The C-CPE-AuNPs complex was generated as followed: The Strep-tagged C-CPE in elution buffer and Strep-Tactin® conjugated AuNPs (diameter 25 nm) (Aurion, Wageningen, Netherlands) were mixed and incubated overnight at 4 °C. The concentration was adjusted to 20 µg/ml C-CPE and 2.5×10^{10} AuNPs/mL with cell culture medium.

In addition to non-treated cells, cells incubated with either non-functionalized AuNPs or C-CPE alone, were used as controls. Cells were exposed to a pulsed laser with 72 mJ/cm² at a scanning speed of 0.5 cm/s. Laser treated cells were incubated for 30 min with 1 µM Hoechst 33258 (Sigma-Aldrich) and 10 min with SYTOX green (1:500, PromoCell GmbH, Heidelberg, Germany) in a cell incubator. Under the Ti-E inverted fluorescence microscope (Nikon, Duesseldorf, Germany), images were taken with 4x objective and Nikon Software Nis-Elements 4.4 (346 nm for Hoechst 33258 and 488 nm for SYTOX green). Vital cells were indicated by Hoechst uptake whereas dead cells were referred by SYTOX and Hoechst uptake. Mean values of three wells were used per experiment. The experiment was performed three times. For cell survival quantification, Hoechst and SYTOX stained cells were counted with the image processing software ImageJ/Fiji V2.0.0.

Electron microscopy

To examine the binding of AuNPs and C-CPE- AuNPs on cell surfaces, the DT0846 and transfected DT0846-FusionRed cell lines were analyzed with scanning electron microscopy (SEM). Confluent cells were treated with AuNPs and C-CPE-AuNPs for 3 h in cell culture incubator to allow complex adhesion to the cells. The cells were exposed to a pulsed laser with 60 mJ/cm² at a scanning speed of 0.5 cm/s. Subsequently, the cells were fixed with 4% formaldehyde, washed with PBS, and stored for further processing. For SEM preparation, the coverslips were dehydrated with a graded series of ethanol completed with an acetone step prior to critical point drying with CO2 as an intermedium (Emitech K850 critical point dryer, Emitech/Quorum Technologies Ltd., Laughton, UK). The coverslips were flat mounted on SEM-stubs with adhesive carbon tape (Plano, Wetzlar, Germany) and coated with a carbon layer (Leica SCD500, Leica Microsystems, Wetzlar Germany). Specimens were analyzed in a field-emission SEM (Zeiss Merlin VP compact, Carl Zeiss Microscopy, Oberkochen, Germany) equipped with HE-SE and in-lens-Duo detectors operated at 5 kV and images with a size of 1024 × 768 pixels were recorded at different steps of magnification.

Statistical analysis

The results are given as mean of at least three independent experiments for quantitative real-time RT-PCR and cell killing using GNOM-LP. Statistical analysis was performed using SAS software 7.1 (SAS Institute Inc., Cary, NC, USA). Significant differences in gene expression of CLDN3, -4 and − 7 were calculated using Student’s two-sided t-test. Statistical analysis of cell killing using GNOME-LP was performed using Dunnett´s Multiple Comparison Test and Student´s two-sided t-test. Differences were considered statistically significant for $p < 0.05$.

Results

Generation of red fluorescent tumor cell lines

Transfected cell lines DT0840-FusionRed and DT0846-FusionRed showed a distinct red fluorescence 24–72 h post-transfection all over the cytoplasm whereas native DT0840 and DT0846 cells showed no

FusionRed fluorescence (Fig. 1A and 1C).

In order to quantify the amount of FusionRed positive cells, both fluorescent cell lines DT0840 and DT0846 were compared to native DT0840 and DT0846 cells by flow cytometry. After 50 passages of geneticin selection, 95.6% and 70.5% of cells were found FusionRed positive in DT0840-FusionRed and DT0846-FusionRed respectively (Fig. 1B and 1D).

In vitro imaging using NightOWL LB 983 *in vivo* imaging system

Transfected DT0840-FusionRed and DT0846-FusionRed cells were further imaged in a NightOWL LB 983 *in vivo* imaging system to illustrate and quantify fluorescent intensity in a whole body imager. Both cell lines showed comparable cell concentration dependent fluorescent intensity. The lower limit of detection was 0.3125×10^6 cells per well with 2.64 average cps ± 3.734 and 4.485 mm² ± 6.343 for DT0840-FusionRed cell line. For DT0846 the lower detection limit was 0.625×10^6 cells per well with 5.69 average cps ± 0.339 and 19.08 mm² ± 5.629 (Fig. 2).

CLDN gene expression in transfected cell lines

Gene expression level of *CLDN3, -4* and *− 7* in transfected cell lines were examined by quantitative real-time RT-PCR and compared to the native cell lines. Level of *CLDN4* expression in DT0840-FusionRed was significantly lower in comparison to the reference cell line (Fig. 3). In contrast, levels of *CLDN3* and *− 4* in DT0846-FusionRed was higher than those of the reference cell line.

CLDN protein immunofluorescence

The presence of CLDN3, -4 and − 7 proteins in native and transfected cell lines were subsequently examined by immunostaining. In DT0840 cell line, CLDN3, -4 and − 7 proteins showed a strong signal and were localized at the cell membranes and in the cytoplasm (Fig. 4). For the DT0840-FusionRed cell line, CLDN3, -4 and − 7 proteins were found at the cell membrane; CLDN7 was weakly expressed (Fig. 4).

Expression of CLDN3 and − 7 proteins in cell line DT0846 was localized at the cell membranes whereas CLDN4 was punctually localized in the cytoplasm and at the cell membrane. In the generated DT0846-FusionRed cell line, CLDN3, -4 and − 7 proteins were strongly distributed along the cell membranes (Fig. 4).

Binding of C-CPE to cell lines

C-CPE's capability to target CLDN was determined through visualization of C-CPE-CLDN binding. The experiment was performed by coupling C-CPE was coupled to Strep-Tactin® Chromeo 488. The complex was detected along cell membranes of native and transfected cell lines at cell-cell junction between adjacent cells (Fig. 5).

Electron microscopy

In order to investigate the binding of AuNPs and C-CPE-AuNPs complexes on the cell surface, DT0846 and transfected DT0846-FusionRed cells were examined by scanning electron microscopy (SEM). AuNPs appearing as white bright spheres in high resolution SEM analysis were detected e.g. on microvilli extending from the cell surfaces of DT0846 and DT0846-FusionRed cells (Fig. 6). Uncoupled AuNPs showed a broad distribution at the cell surface while C-CPE AuNPs were found preferentially located in close distance to cell-cell borders. Whereas the presence of AuNPs and C-CPE-AuNPs on microvilli may indicate non-specific surface binding, at places internalization of AuNPs was clearly visible (see Additional file 1).

Selective cancer cells ablation using GNOME-LP and C-CPE-AuNPs complex

Laser exposure of DT0840 native and transfected CLDN expressing cells in combination with C-CPE functionalized AuNPs significantly reduced amount of vital cells down to 32.73% and 26.86% respectively in comparison to untreated cells (Fig. 7). In native and transfected DT0846 cell lines in comparison to untreated cells, GNOME-LP in combination with C-CPE functionalized AuNPs significantly decreased cell survival to 8.55% and 5.52% respectively.

In cells treated with C-CPE alone, GNOME-LP application did not significantly impair cell survival. Application of GNOME-LP in presence of non-functionalized AuNPs reduced cells by 41.56% of DT0840 and 30.91% of DT0840-FusionRed cells. Similarly, laser exposure of DT0846 and DT0846-FusionRed in combination with non-functionalized AuNPs significantly decreased cells survival to 69.81% and 70.76% respectively. Killing efficiency in presence of functionalized AuNPs (C-CPE + AuNPs) was significantly higher in comparison to killing with non-functionalized AuNPs.

Discussion

In vivo models are the key to understand the pathogenesis of prostate cancer and the development of novel therapeutic approaches [2]. Although *in vitro* systems offer several possibilities for basic drug evaluation, they remain limited for the evaluation of complex interactions. The use of long-wavelength emitting fluorescent proteins to label cancer cells enables deep tissue imaging; thereby allow real-time tracing of cancer growth, metastasis and determination of efficacy of candidate antitumor and anti-metastatic therapies. An optimal fluorescent protein for whole-body imaging should have excitation and emission spectra within 650–950 nm. This “near-infrared optical window” has the lowest absorbance by hemoglobin, melanin and water in mammalian tissue [9].

Herein, two canine prostate cancer cell lines, stably expressing red fluorescent protein, were established. These cell lines can be detected in living animals using fluorescence imaging systems. The generated cells have shown stable long time expression of red fluorescent protein; therefore represent a valuable tool for studying canine prostate cancer *in vivo* models such as xenograft mice.

It is well documented that CPE receptors CLDN3, -4 and/or -7 are abnormally regulated in many tumor types [10–13, 49, 50], which also was confirmed for the used 0840 and 0846 cell lines [41]. CLDN3, -4 and − 7 expressions in generated fluorescent cell line DT0840-FusionRed revealed no significant difference in comparison to native DT0840 for *CLDN3* and *− 7*, however CLDN4 was significantly decreased. Analysis of *CLDN7* in DT0846-FusionRed showed no difference in expression, whereas *CLDN3* and *− 4* were even higher expressed after transfection.

Immunofluorescence staining showed strong expression of all three CLDN proteins in all cell lines. Therefore, DT0840-FusionRed still represents a sufficient model for further experiments despite significant decrease in *CLDN4* mRNA level measured by qPCR. Interestingly, immunofluorescence staining revealed that CLDN3, -4 and − 7 in DT0840 cells, as well as CLDN4 in DT0846, were punctually located in the cytoplasm. Such apparent miss-localizations were also described for the CLDN4 protein in human prostate cancer-derived cell lines and may be related to loss of cellular organization due to a defect in tight junction formation or cell polarity; features common in tumor cells [43].

Binding of CPE to CLDN3 and − 4 can trigger cell death [51–54]. Therefore, it proposed to use CPE for tumor therapy. However, studies *in vivo* revealed that systemic administration of full-length CPE in mice was toxic and thus limited its use to local therapies [52]. Previously we demonstrated that the non-cytotoxic C-terminal domain of CPE, which preserves CPE's binding affinity to CLDN receptors, is capable to functionalize AuNPs [36]. Imaging of C-CPE binding to the canine tumor cell lines proved that the protein can specifically target CLDN3, -4 and − 7 demonstrating that the functionalization did not alter the binding capacity to CLDN.

Further, electron microscopy images indicated that the C-CPE conjugated AuNPs retain the affinity to its receptors (CLDN3, -4 and − 7).

The GNOME-LP technology has been used for the cellular introduction of dyes as well as siRNA into different cell types via transient cell permeabilization [55–58]. The present report shows that C-CPE coupled to Strep-Tactin conjugated AuNPs in combination with GNOME-LP technique can be used for specific targeting of CLDNs expressing tumor cell lines.

In the previous study, we showed that the energy power of the applied laser at 60 mJ/cm^3 and a scanning speed of 0.5 cm/s in combination with C-CPE-AuNPs reduced cell survival to less than 30% of claudin expressing cell lines [36]. In a first experiment, GNOME-LP with the same settings accordingly reduced cell survival to about 30% in native DT0846 cells, but showed no effect on the transfected fluorescence cells (data not shown). At 532 nm (laser wavelength) the red fluorescent dye FusionRed has approx. 50% absorption (50% of dye molecules absorb light at 532 nm). Therefore, depending on dye concentration in the cells, a significant amount of laser light might be absorbed and thus reduced the overall effect on AuNPs. Therefore, GNOME-LP was applied at the maximal laser fluence (72 mJ/cm^3) on native and fluorescent cell lines. Using the new setting, GNOME-LP in combination with C-CPE functionalized AuNPs

reduced cell survival to down to 30% in DT0840 and less than 10% in DT0846 (native and fluorescent) cells.

Significant killing of DT0846 and DT0840 (native and transfected) cells treated with non-functionalized AuNPs may be related to endocytosis activity allowing them to internalize the AuNPs. However, the results show that the functionalization of AuNPs with C-CPE increases the ablation efficiency of CLDN expressing tumor cell lines in comparison to cells treated only with AuNPs. This interpretation is supported by SEM analysis showing the presence of many uncoupled AuNPs that are bound non-specifically on the cell surface microvilli even after three hours of incubation whereas fewer C-CPE functionalized AuNPs are present on the cell surface, mostly restricted along cell-cell borders. This suggests that C-CPE-AuNPs efficiently bind to their protein targets and are rapidly internalized into the cells as can be traced at places with SEM (see Additional file 1).

In the current study, the generated DT0840-FusionRed and DT0846-FusionRed cell lines showed stably strong red fluorescence protein expression. This was further analyzed by NightOWL LB 983 *in vivo* imaging system, where the fluorescent detection potential of FusionRed transfected DT0840 and DT0846 cell lines were verified. Small cell numbers were sufficient to monitor the FusionRed labeled cells in the whole body imager [59]. For *in vivo* imaging studies a cell number from 1×10^6 cells per tumor is detectable with this setting already in early tumor stages [60]. Red fluorescent proteins showed high sensitivity in subcutaneous, abdominal as well as deep tissue cell implantation. Thus, *in vivo* imaging with this stably transfected cell lines provides a tool for long-term imaging and monitoring longitudinal tumor development and drug response per individual mouse [61].

The results confirm for the first time that the therapy concept of C-CPE functionalized AuNPs can be used efficiently against prostate carcinoma cells. By using GNOME-LP system and C-CPE functionalized AuNPs an irreversible laser ablation of prostate tumor cells was achieved *in vitro*. Cells, which were irradiated with maximal laser power without C-CPE-AuNPs, maintained viability. Likewise, cells incubated with C-CPE and irradiated with the maximal laser fluence maintained viability as well. A combination of laser treatment and C-CPE-AuNPs, however, reduced tumor cell viability down to less than 10% in DT0846.

To further extend the presented *in vitro* findings, *in vivo* studies need to be carried out in a next step. The same cell lines used for the *in vitro* findings can also be detected *in vivo* through deep tissue imaging and therefore enabling to observe tumor growth and subsequently possible tumor ablation through C-CPE treatment in a living animal e.g. mouse xenograft models. *In vivo* studies could allow the characterization if the C-CPE complex is able to diffuse through the extracellular matrix and bind to tumor tissues. If successful, a combination between GNOME-LP and functionalized AuNPs may establish a treatment option for canine prostate cancer.

Conclusion

The established cell lines and the verified proof of concept *in vitro* provide the basis for perspective xenograft *in vivo* studies. The introduced red fluorescence enables deep tissue imaging in living animals and therefore detailed characterization of tumor growth and subsequently possible tumor ablation through C-CPE-AuNPs treatment.

Since dogs represent an excellent model for prostate cancer, the development of therapeutic strategies provides an important contribution to translational research directed to treat humans, thus providing benefit for both species.

Abbreviations

CLDN: Claudin; C-CPE: C-terminus of Clostridium perfringens enterotoxin; AuNPs: gold nanoparticles; RFP: Red fluorescent protein; GNOME-LP: gold nanoparticle mediated laser perforation; G418: Geneticin, SEM: Scanning electron microscopy.

Declarations

Ethics approval and consent to participate

Not applicable

Consent for publication

Not applicable

Availability of data and materials

All data generated or analyzed during the current study are included in this publication and its supplementary information files without restriction.

Competing interests

The authors declare that they have no competing interests.

Funding

The Authors wish to thanks Aleppo University and HGFK (Hannoversche Gesellschaft zur Förderung der Kleintiermeidizin e.V.) for supporting SA with a scholarship.

Authors' Contributions

S.A., I.N. and H.M.E. performed the conception of the experiments; J.T.S., A.N., A.B., I.N. and H.M.E. performed the manuscript revision and editing; A.B. performed cell killing, C-CPE Binding and immunofluorescences experiments; S.S. and S.V.P performed in vitro imaging using the NightOWL LB

983; M.F. performed electron microscopy; S.A. and T.K. performed the transfection of cell lines; S.A. and J.T.S. performed statistical analysis; S.A. performed the cell cultivation, flow cytometry, immunofluorescences analysis, RNA isolation, qPCR, and analyzed the data and wrote the paper.

Acknowledgements

The authors would like to thank Prof. Dr. Alexander Heisterkamp, Institute of Quantum Optics, Leibniz University Hannover for cell killing data interpretation and Karoline Schulz and Dr. Armin Springer, Medical Biology and Electron Microscopy Centre, University of Rostock for technical support during electron microscopy analysis.

References

1. Rutgen BC, Willenbrock S, Reimann-Berg N, Walter I, Fuchs-Baumgartinger A, Wagner S, et al. Authentication of primordial characteristics of the CLBL-1 cell line prove the integrity of a canine B-cell lymphoma in a murine in vivo model. PLoS One. 2012;7(6):e40078.
2. Cunningham D, You Z. In vitro and in vivo model systems used in prostate cancer research. J Biol Methods. 2015;2(1).
3. Hoffman RM. The multiple uses of fluorescent proteins to visualize cancer in vivo. Nat Rev Cancer. 2005;5(10):796-806.
4. Hoffman RM, Yang M. Whole-body imaging with fluorescent proteins. Nat Protoc. 2006;1(3):1429-38.
5. Shcherbo D, Shemiakina, II, Ryabova AV, Luker KE, Schmidt BT, Souslova EA, et al. Near-infrared fluorescent proteins. Nat Methods. 2010;7(10):827-9.
6. Luker KE, Pata P, Shemiakina, II, Pereverzeva A, Stacer AC, Shcherbo DS, et al. Comparative study reveals better far-red fluorescent protein for whole body imaging. Sci Rep. 2015;5:10332.
7. Hoffman RM. The Advantages of Using Fluorescent Proteins for In Vivo Imaging. Current Protocols Essential Laboratory Techniques. 2017;15(1):9.6.1-9.6.24.
8. Shcherbo D, Merzlyak EM, Chepurnykh TV, Fradkov AF, Ermakova GV, Solovieva EA, et al. Bright far-red fluorescent protein for whole-body imaging. Nat Methods. 2007;4(9):741-6.
9. Shcherbakova DM, Subach OM, Verkhusha VV. Red fluorescent proteins: advanced imaging applications and future design. Angew Chem Int Ed Engl. 2012;51(43):10724-38.
10. Furuse M, Fujita K, Hiiragi T, Fujimoto K, Tsukita S. Claudin-1 and -2: novel integral membrane proteins localizing at tight junctions with no sequence similarity to occludin. J Cell Biol. 1998;141(7):1539-50.
11. Jakab C, Halasz J, Szasz AM, Kiss A, Schaff Z, Rusvai M, et al. Expression of claudin-1, -2, -3, -4, -5 and -7 proteins in benign and malignant canine mammary gland epithelial tumours. J Comp Pathol. 2008;139(4):238-45.
12. Jakab C, Rusvai M, Galfi P, Szabo Z, Szabara A, Kulka J. Expression of claudin-1, -3, -4, -5 and -7 proteins in low grade colorectal carcinoma of canines. Histol Histopathol. 2010;25(1):55-62.

13. Jakab CS, Rusvai M, Demeter Z, Galfi P, Szabo Z, Kulka J. Expression of claudin-4 molecule in canine exocrine pancreatic acinar cell carcinomas. Histol Histopathol. 2011;26(9):1121-6.
14. Kominsky SL, Argani P, Korz D, Evron E, Raman V, Garrett E, et al. Loss of the tight junction protein claudin-7 correlates with histological grade in both ductal carcinoma in situ and invasive ductal carcinoma of the breast. Oncogene. 2003;22(13):2021-33.
15. Krajewska M, Olson AH, Mercola D, Reed JC, Krajewski S. Claudin-1 immunohistochemistry for distinguishing malignant from benign epithelial lesions of prostate. Prostate. 2007;67(9):907-10.
16. Krause G, Winkler L, Mueller SL, Haseloff RF, Piontek J, Blasig IE. Structure and function of claudins. Biochim Biophys Acta. 2008;1778(3):631-45.
17. Furuse M, Sasaki H, Fujimoto K, Tsukita S. A single gene product, claudin-1 or -2, reconstitutes tight junction strands and recruits occludin in fibroblasts. J Cell Biol. 1998;143(2):391-401.
18. Furuse M, Sasaki H, Tsukita S. Manner of interaction of heterogeneous claudin species within and between tight junction strands. J Cell Biol. 1999;147(4):891-903.
19. Tsukita S, Furuse M. Occludin and claudins in tight-junction strands: leading or supporting players? Trends Cell Biol. 1999;9(7):268-73.
20. Fujita K, Katahira J, Horiguchi Y, Sonoda N, Furuse M, Tsukita S. Clostridium perfringens enterotoxin binds to the second extracellular loop of claudin-3, a tight junction integral membrane protein. FEBS Lett. 2000;476(3):258-61.
21. Katahira J, Inoue N, Horiguchi Y, Matsuda M, Sugimoto N. Molecular cloning and functional characterization of the receptor for Clostridium perfringens enterotoxin. J Cell Biol. 1997;136(6):1239-47.
22. Sonoda N, Furuse M, Sasaki H, Yonemura S, Katahira J, Horiguchi Y, et al. Clostridium perfringens enterotoxin fragment removes specific claudins from tight junction strands: Evidence for direct involvement of claudins in tight junction barrier. J Cell Biol. 1999;147(1):195-204.
23. Veshnyakova A, Piontek J, Protze J, Waziri N, Heise I, Krause G. Mechanism of Clostridium perfringens enterotoxin interaction with claudin-3/-4 protein suggests structural modifications of the toxin to target specific claudins. J Biol Chem. 2012;287(3):1698-708.
24. Kokai-Kun JF, McClane BA. Deletion analysis of the Clostridium perfringens enterotoxin. Infect Immun. 1997;65(3):1014-22.
25. Kondoh M, Masuyama A, Takahashi A, Asano N, Mizuguchi H, Koizumi N, et al. A novel strategy for the enhancement of drug absorption using a claudin modulator. Mol Pharmacol. 2005;67(3):749-56.
26. Markman M. Intraperitoneal antineoplastic drug delivery: rationale and results. Lancet Oncol. 2003;4(5):277-83.
27. Abadeer NS, Murphy CJ. Recent Progress in Cancer Thermal Therapy Using Gold Nanoparticles. The Journal of Physical Chemistry C. 2016;120(9):4691-716.
28. Chen Q, Chen Q, Qi H, Ruan L, Ren Y. Experimental Comparison of Photothermal Conversion Efficiency of Gold Nanotriangle and Nanorod in Laser Induced Thermal Therapy. Nanomaterials.

2017;7(12):416.
29. Jain S, Hirst DG, O'Sullivan JM. Gold nanoparticles as novel agents for cancer therapy. Br J Radiol. 2012;85(1010):101-13.
30. Fekrazad R, Naghdi N, Nokhbatolfoghahaei H, Bagheri H. The Combination of Laser Therapy and Metal Nanoparticles in Cancer Treatment Originated From Epithelial Tissues: A Literature Review. J Lasers Med Sci. 2016;7(2):62-75.
31. Norouzi H, Khoshgard K, Akbarzadeh F. In vitro outlook of gold nanoparticles in photo-thermal therapy: a literature review. Lasers Med Sci. 2018;33(4):917-26.
32. Ashiq MG, Saeed MA, Tahir BA, Ibrahim N, Nadeem M. Breast cancer therapy by laser-induced Coulomb explosion of gold nanoparticles. Chin J Cancer Res. 2013;25(6):756-61.
33. Liu SY, Liang ZS, Gao F, Luo SF, Lu GQ. In vitro photothermal study of gold nanoshells functionalized with small targeting peptides to liver cancer cells. J Mater Sci Mater Med. 2010;21(2):665-74.
34. Bartczak D, Muskens OL, Millar TM, Sanchez-Elsner T, Kanaras AG. Laser-induced damage and recovery of plasmonically targeted human endothelial cells. Nano Lett. 2011;11(3):1358-63.
35. Li X, Zhou H, Yang L, Du G, Pai-Panandiker AS, Huang X, et al. Enhancement of cell recognition in vitro by dual-ligand cancer targeting gold nanoparticles. Biomaterials. 2011;32(10):2540-5.
36. Becker A, Leskau M, Schlingmann-Molina BL, Hohmeier SC, Alnajjar S, Murua Escobar H, et al. Publisher Correction: Functionalization of gold-nanoparticles by the Clostridium perfringens enterotoxin C-terminus for tumor cell ablation using the gold nanoparticle-mediated laser perforation technique. Sci Rep. 2019;9(1):4150.
37. Becker A, Lehrich T, Kalies S, Heisterkamp A, Ngezahayo A. Parameters for Optoperforation-Induced Killing of Cancer Cells Using Gold Nanoparticles Functionalized With the C-terminal Fragment of Clostridium Perfringens Enterotoxin. Int J Mol Sci. 2019;20(17).
38. Waters DJ, Sakr WA, Hayden DW, Lang CM, McKinney L, Murphy GP, et al. Workgroup 4: spontaneous prostate carcinoma in dogs and nonhuman primates. Prostate. 1998;36(1):64-7.
39. MacEwen EG. Spontaneous tumors in dogs and cats: models for the study of cancer biology and treatment. Cancer Metastasis Rev. 1990;9(2):125-36.
40. Keller JM, Schade GR, Ives K, Cheng X, Rosol TJ, Piert M, et al. A novel canine model for prostate cancer. Prostate. 2013;73(9):952-9.
41. Hammer SC, Nagel S, Junginger J, Hewicker-Trautwein M, Wagner S, Heisterkamp A, et al. Claudin-1, -3, -4 and -7 gene expression analyses in canine prostate carcinoma and mammary tissue derived cell lines. Neoplasma. 2016;63(2):231-8.
42. Kominsky SL. Claudins: emerging targets for cancer therapy. Expert Rev Mol Med. 2006;8(18):1-11.
43. Landers KA, Samaratunga H, Teng L, Buck M, Burger MJ, Scells B, et al. Identification of claudin-4 as a marker highly overexpressed in both primary and metastatic prostate cancer. Br J Cancer. 2008;99(3):491-501.

44. Long H, Crean CD, Lee WH, Cummings OW, Gabig TG. Expression of Clostridium perfringens enterotoxin receptors claudin-3 and claudin-4 in prostate cancer epithelium. Cancer Res. 2001;61(21):7878-81.
45. Sheehan GM, Kallakury BV, Sheehan CE, Fisher HA, Kaufman RP, Jr., Ross JS. Loss of claudins-1 and -7 and expression of claudins-3 and -4 correlate with prognostic variables in prostatic adenocarcinomas. Hum Pathol. 2007;38(4):564-9.
46. Sun F, Baez-Diaz C, Sanchez-Margallo FM. Canine prostate models in preclinical studies of minimally invasive interventions: part I, canine prostate anatomy and prostate cancer models. Transl Androl Urol. 2017;6(3):538-46.
47. Reimann-Berg N, Willenbrock S, Murua Escobar H, Eberle N, Gerhauser I, Mischke R, et al. Two new cases of polysomy 13 in canine prostate cancer. Cytogenet Genome Res. 2011;132(1-2):16-21.
48. Harting T, Stubbendorff M, Willenbrock S, Wagner S, Schadzek P, Ngezahayo A, et al. The effect of dichloroacetate in canine prostate adenocarcinomas and transitional cell carcinomas in vitro. Int J Oncol. 2016;49(6):2341-50.
49. Escudero-Esparza A, Jiang WG, Martin TA. The Claudin family and its role in cancer and metastasis. Front Biosci (Landmark Ed). 2011;16:1069-83.
50. Michl P, Buchholz M, Rolke M, Kunsch S, Lohr M, McClane B, et al. Claudin-4: a new target for pancreatic cancer treatment using Clostridium perfringens enterotoxin. Gastroenterology. 2001;121(3):678-84.
51. Gao Z, McClane BA. Use of Clostridium perfringens Enterotoxin and the Enterotoxin Receptor-Binding Domain (C-CPE) for Cancer Treatment: Opportunities and Challenges. J Toxicol. 2012;2012:981626.
52. Kominsky SL, Vali M, Korz D, Gabig TG, Weitzman SA, Argani P, et al. Clostridium perfringens enterotoxin elicits rapid and specific cytolysis of breast carcinoma cells mediated through tight junction proteins claudin 3 and 4. Am J Pathol. 2004;164(5):1627-33.
53. McClane BA. The complex interactions between Clostridium perfringens enterotoxin and epithelial tight junctions. Toxicon. 2001;39(11):1781-91.
54. Kitadokoro K, Nishimura K, Kamitani S, Fukui-Miyazaki A, Toshima H, Abe H, et al. Crystal structure of Clostridium perfringens enterotoxin displays features of beta-pore-forming toxins. J Biol Chem. 2011;286(22):19549-55.
55. Baumgart J, Bintig W, Ngezahayo A, Willenbrock S, Murua Escobar H, Ertmer W, et al. Quantified femtosecond laser based opto-perforation of living GFSHR-17 and MTH53 a cells. Opt Express. 2008;16(5):3021-31.
56. Begandt D, Bader A, Antonopoulos GC, Schomaker M, Kalies S, Meyer H, et al. Gold nanoparticle-mediated (GNOME) laser perforation: a new method for a high-throughput analysis of gap junction intercellular coupling. J Bioenerg Biomembr. 2015;47(5):441-9.
57. Heinemann D, Schomaker M, Kalies S, Schieck M, Carlson R, Murua Escobar H, et al. Gold nanoparticle mediated laser transfection for efficient siRNA mediated gene knock down. PLoS One. 2013;8(3):e58604.

58. Kalies S, Heinemann D, Schomaker M, Gentemann L, Meyer H, Ripken T. Immobilization of gold nanoparticles on cell culture surfaces for safe and enhanced gold nanoparticle-mediated laser transfection. J Biomed Opt. 2014;19(7):70505.
59. Zhu H, Kauffman ME, Trush MA, Jia Z, Li YR. A Simple Bioluminescence Imaging Method for Studying Cancer Cell Growth and Metastasis after Subcutaneous Injection of Lewis Lung Carcinoma Cells in Syngeneic C57BL/6 Mice. React Oxyg Species (Apex). 2018;5(14):118-25.
60. Zhou K, Ding Y, Vuletic I, Tian Y, Li J, Liu J, et al. In vivo long-term investigation of tumor bearing mKate2 by an in-house fluorescence molecular imaging system. Biomed Eng Online. 2018;17(1):187.
61. Liang L, Yue Z, Du W, Li Y, Tao H, Wang D, et al. Molecular Imaging of Inducible VEGF Expression and Tumor Progression in a Breast Cancer Model. Cell Physiol Biochem. 2017;42(1):407-15.

Figures

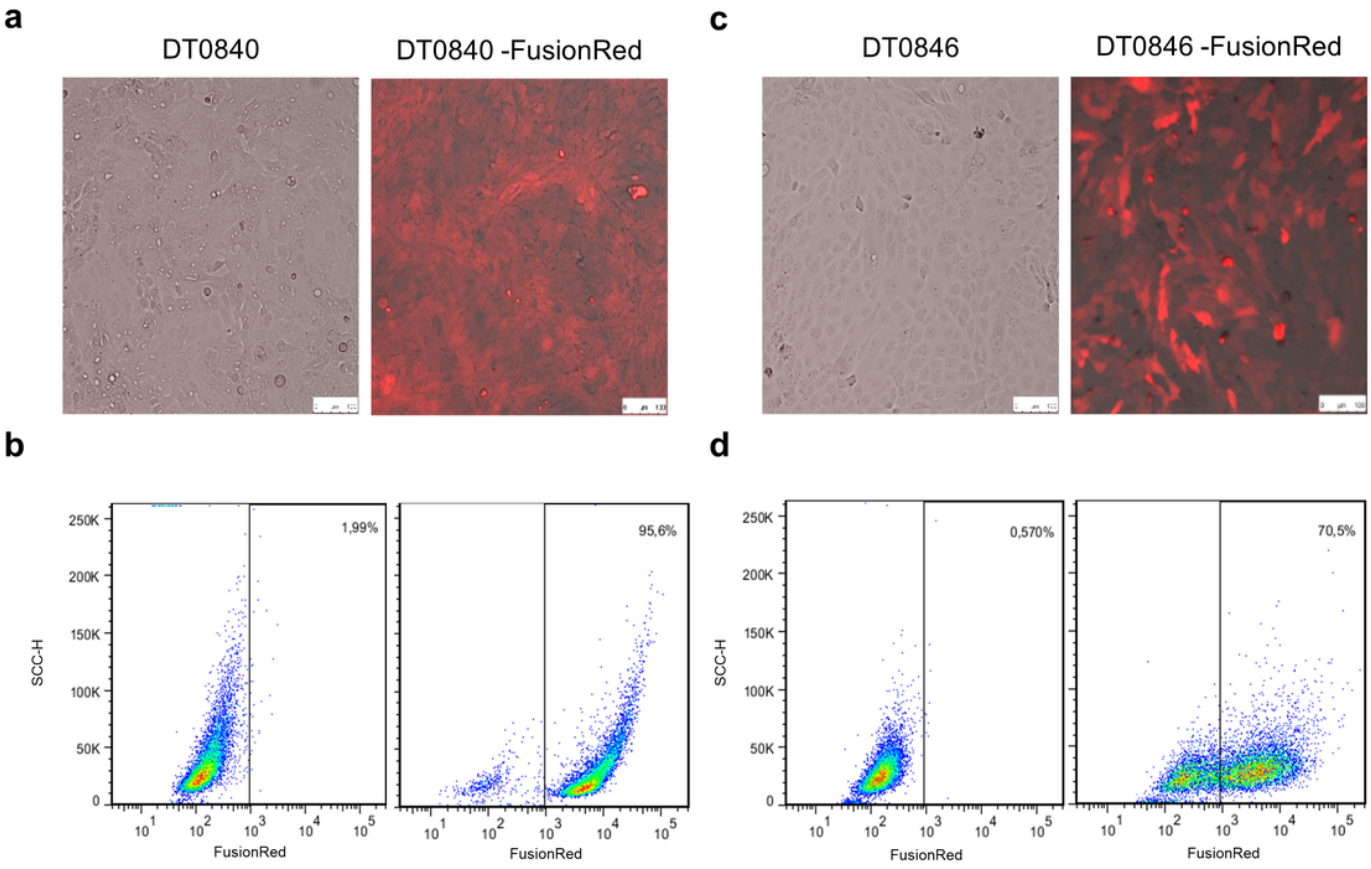

Figure 1

Fluorescence microscopy and flow cytometry analyses of transfected DT0840 and DT0846 cell lines. (a, c) Merged transmitted light and red fluorescence image of FusionRed expressing cells; FusionRed is localized in the cytoplasm. (b, d) Flow cytometric analyses of FusionRed expression in native and fluorescent cell lines depicted in dot-plots showing side scatter (SSC) vs. FusionRed fluorescence.

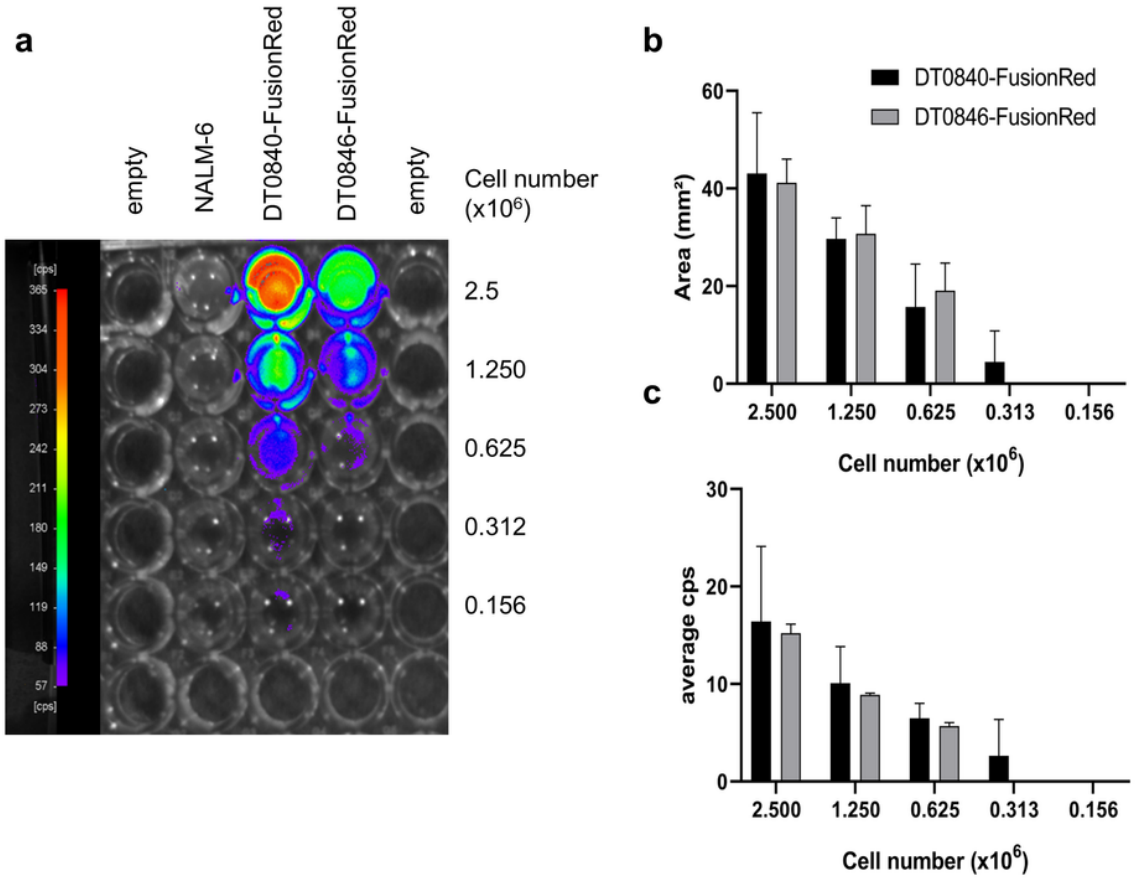

Figure 2

Imaging of transfected DT0840 and DT0846 cell lines using NightOWL LB983 in vivo imaging system. Serial diluted FusionRed labeled DT0840 and DT0846 cells were seeded in a 96 well plate overnight. (a) Subsequently, images were taken using filter with excitation of 525 nm and emission of 655 nm and 10 seconds exposure using the NightOWL LB 983 in vivo imaging system. Pre-B-ALL cell line NALM-6 was used as unlabeled control cell line. (b) Area (mm²) and (c) average counts per seconds (cps) were evaluated by IndiGO software for both cell lines. Error bars represent the mean ± standard deviation (SD).

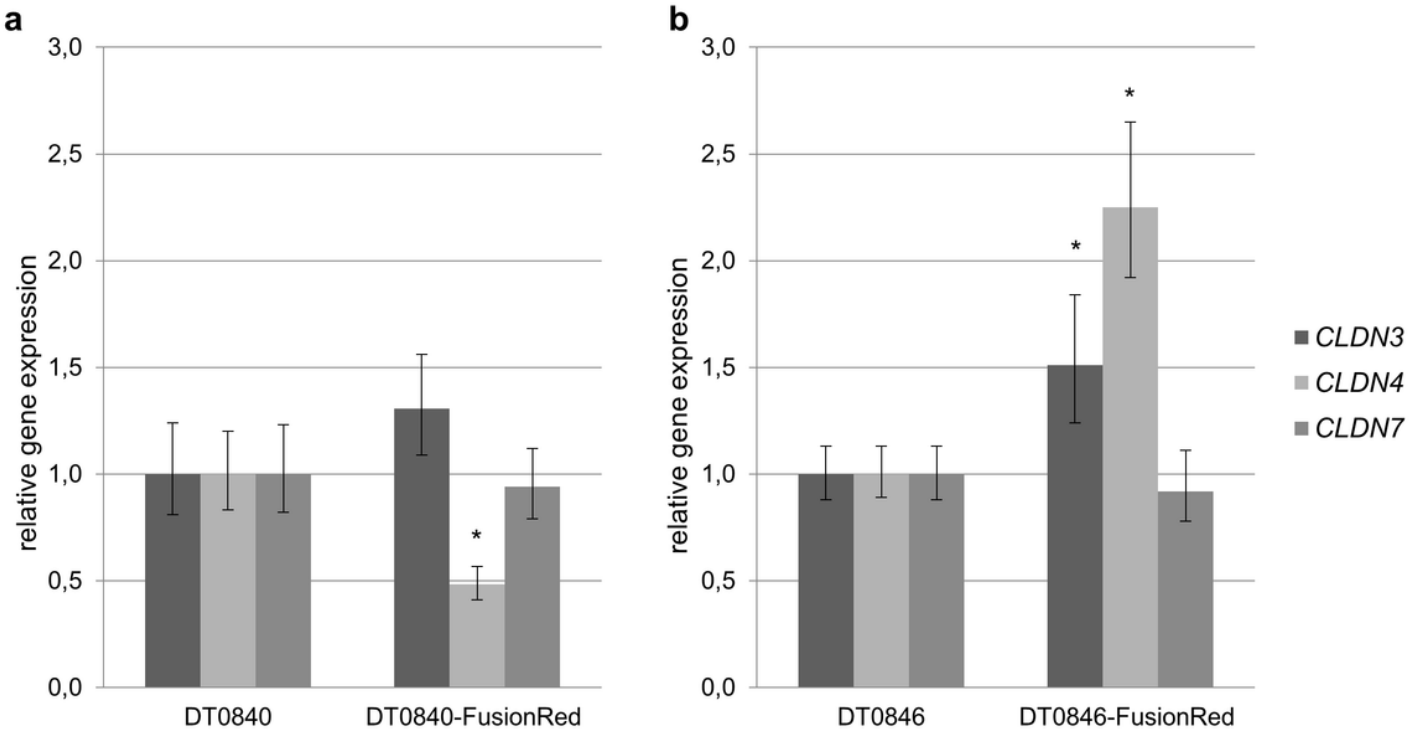

Figure 3

CLDN3, -4 and -7 gene expression in transfected tumor cell lines. Gene expression was measured via quantitative real-time RT-PCR and results were normalized to the expression of GAPDH and ACTB. (a) CLDN gene expression in DT0840-Fusionred in comparison to native DT0840. (b) CLDN gene expression in DT0846-Fusionred in comparison to native DT0846. Error bars represent the mean ± standard deviation (SD). *p<0.05 indicates statistically significant differential expression of CLDN compared to non-transfected cell lines.

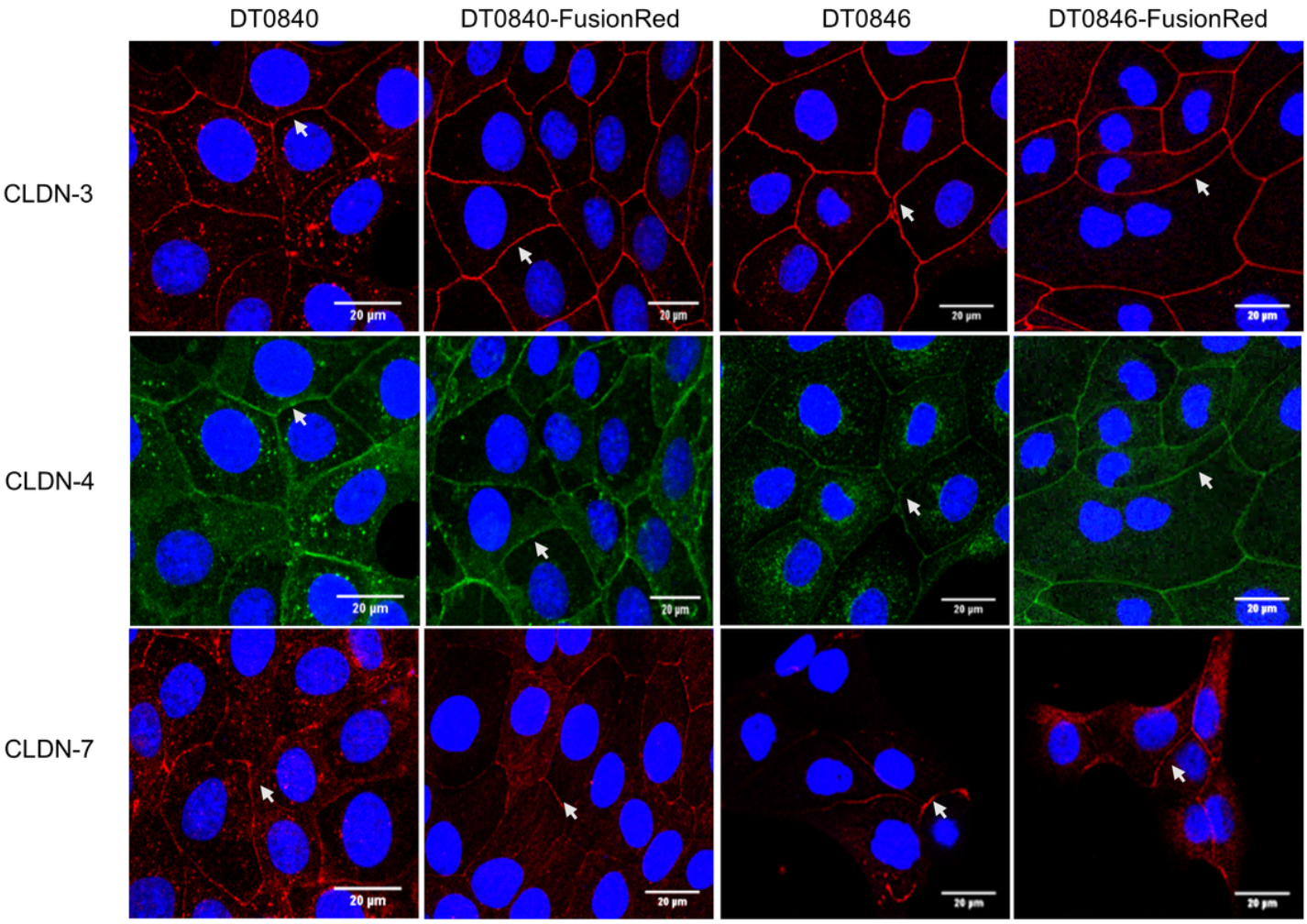

Figure 4

Expression of CLDNs protein in native and transfected tumor cell lines. Cells were subjected to immunostaining with corresponding antibodies using fluorescein-conjugated secondary antibodies, showing red signals for CLDN3 and -7 and green signals for CLDN4. DAPI was used for blue nuclei staining. Images were observed under confocal microscopy. Arrows indicate CLDN localization on cell-cell contact. Scale bars = 20 µm.

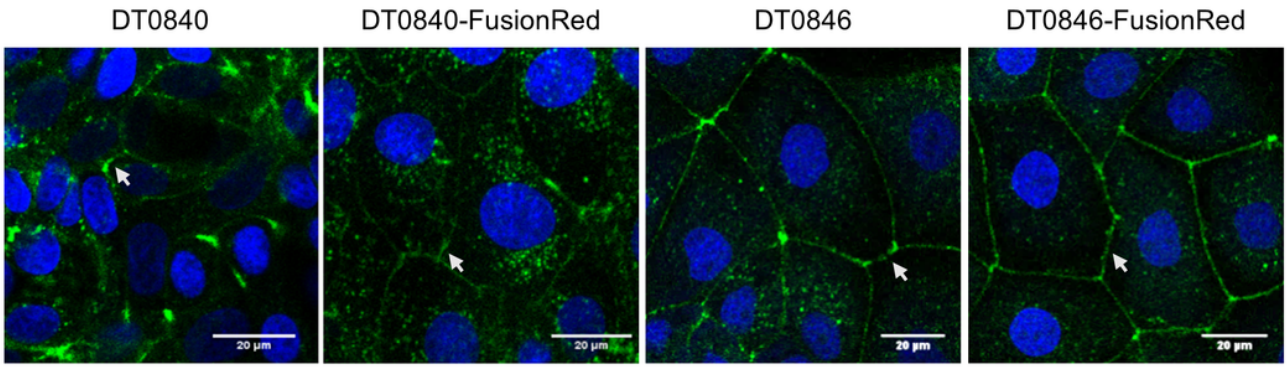

Figure 5

Binding of C-CPE to CLDN. Specific binding of C-CPE-Strep-Tactin Chromeo 488 complex on CLDN expressing cells at cell-cell contact (green). Images were observed under confocal microscopy .Arrows indicate C-CPE binding on cell-cell contact. Scale bars = 20 µm.

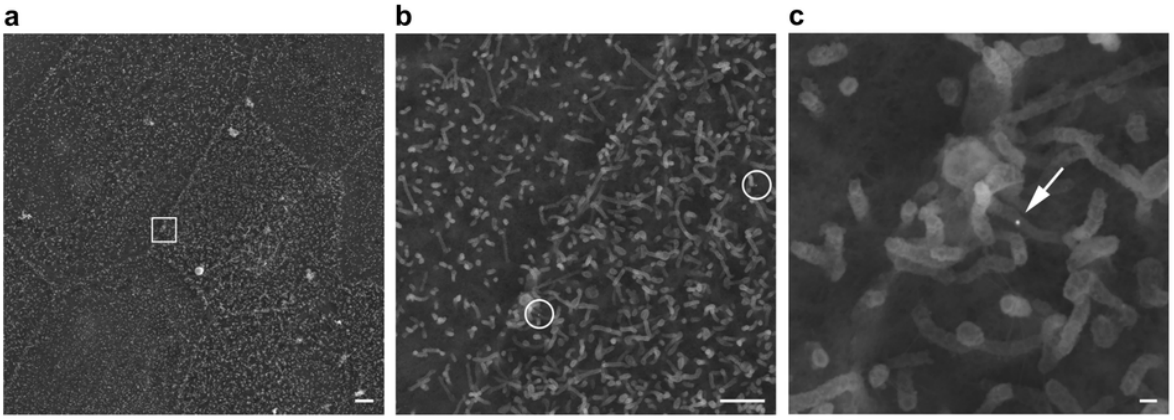

Figure 6

Scanning electron microscopy of C-CPE-AuNPs on a DT0846-FusionRed cell. (a) 2,000x overview of the cell culture and stepwise higher magnification of a cell-cell border area presented in (b) 10,000x with AuNPs encircled and (c) 40,000x detailing an 25nm AuNP (arrow) on surface microvilli. The white box outlined in (a) indicates the area magnified in C Scale bars are 2 µm, 1µm and 100 nm, respectively.

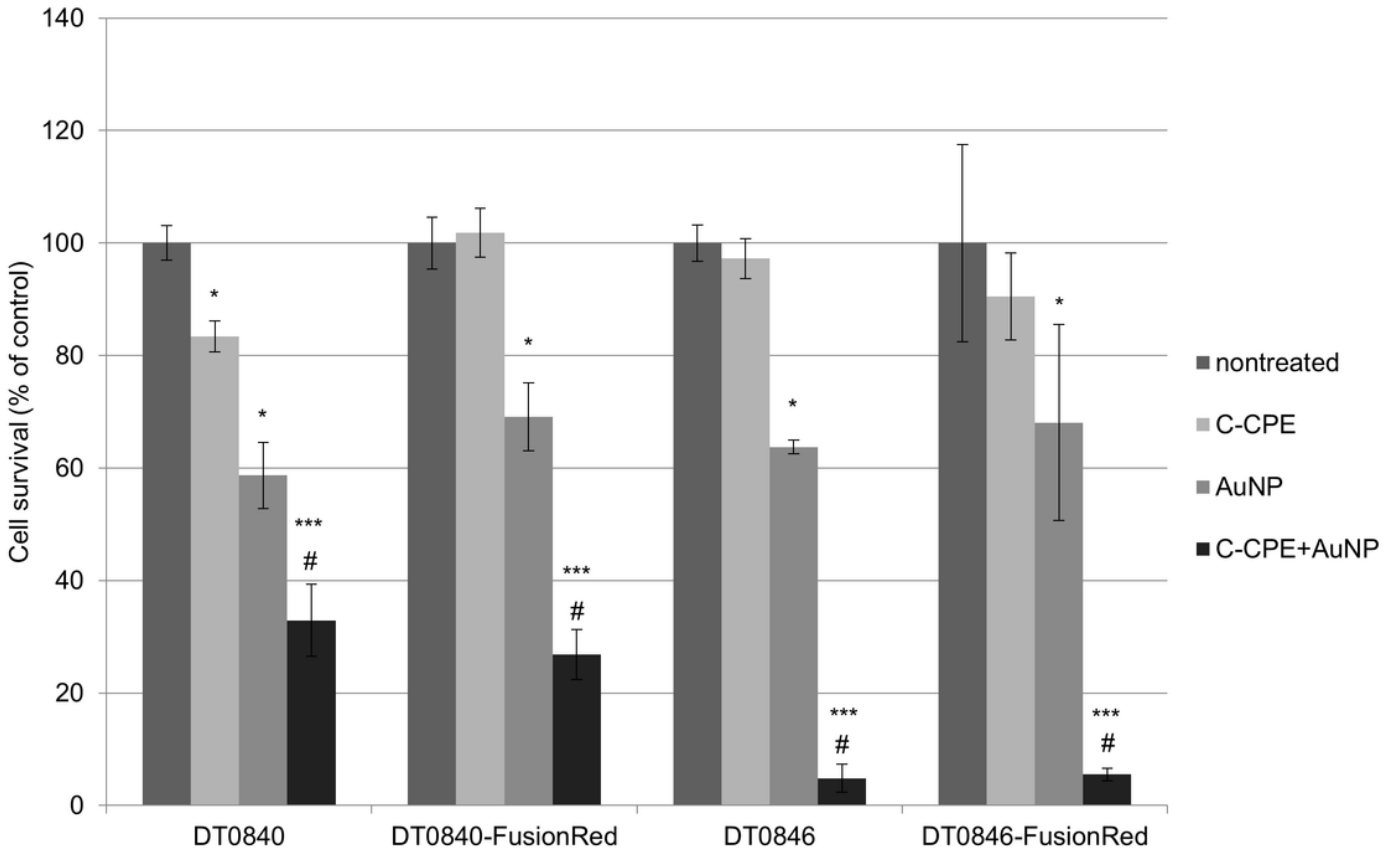

Figure 7

GNOME-LP mediated tumor cell killing using C-CPE functionalized AuNPs. Increased cell killing efficiency of GNOME-LP in presence of C-CPE-AuNPs compared to GNOME-LP in combination with non-functionalized AuNPs. SYTOX green uptake was used as an indicator of cell death after GNOME-LP application. The graph represents the mean ± standard deviation (SD) of cell survival relative to untreated cells as a control reference. Significant differences to untreated controls were analyzed with Student's test. *: $p<0.05$; **: $p<0.01$; ***: $p<0.001$, # Significant difference to cells treated with AuNPs only; $p<0.001$.

Supplementary Files

This is a list of supplementary files associated with this preprint. Click to download.

- Additionalfile1.tif
- Additionalfile2.tif